Applied Catalysis B: Environmental 127 (2012) 148–158

Contents lists available at SciVerse ScienceDirect

Applied Catalysis B: Environmental

journal homepage: www.elsevier.com/locate/apcatb

Nitrate reduction by maghemite supported Cu-Pd bimetallic catalyst

Junyoung Jung, Sungjun Bae, Woojin Lee*

Department of Civil and Environmental Engineering, Korea Advanced Institute of Science and Technology, 291 Daehak-ro, Yuseong-Gu, Daejeon 305-701, Republic of Korea

ARTICLE INFO

Article history:
Received 22 May 2012
Received in revised form 13 August 2012
Accepted 17 August 2012
Available online 25 August 2012

Keywords:
Maghemite
Bimetallic catalyst
Catalytic nitrate reduction
Nitrogen gas selectivity

ABSTRACT

We have investigated the catalytic nitrate reduction by maghemite supported Cu-Pd bimetallic catalyst (maghemite/Cu/Pd). BET, XRD, XPS, TPR, SEM/EDX, TEM analysis were carried out to characterize maghemite/Cu/Pd. Remarkable nitrate removal (99.5%) by maghemite/Cu/Pd was observed in 90 min, while Cu-Pd catalyst supported with alumina (43%) and hematite (63%) showed less efficient nitrate removal. Nitrate removal was excellent (>95%) in all Cu loading variation (0.25–1 wt.%) on maghemite/Cu/Pd, while selectivity of nitrogen gas formed during the reaction was the highest (43%) at a specific Cu/Pd ratio (0.5/0.5 wt.%). We also observed excellent nitrate removals (>95 and >94%, respectively) by maghemite/Cu/Pd in the ranges of Pd loading (0.25–1 wt.%) and hydrogen flow rate (100–500 cc/min). The highest nitrogen selectivities (47 and 45%) were obtained by low Pd loading (0.25 wt.%) and hydrogen flow rate (200 cc/min). Maghemite/Cu/Pd showed slow decrease of nitrate removal (99.5–83%) and low metal leaching (1.5% of Cu leaching) during three reaction cycles. XPS analysis revealed that Cu(0) was oxidized to Cu_2O and CuO during the catalytic nitrate reduction, while Pd(0) was not changed.

1. Introduction

Increased groundwater contamination by nitrate has received an attention in all over the world [1–3] due to intensive use of fertilizer from agricultural activities [4,5], disposal of massive amount of livestock manure [5], and discharge of poorly treated wastewater [6]. Nitrate has been known to be hazardous to human health, which can cause methaemoglobinaemia and blue baby syndrome, fatal disease to babies under 6 months of age, [7] and lead to formation of carcinogenic nitrosamine in the human body [8]. In the efforts to control nitrate contamination in groundwater, United States Environmental Protection Agency and European Community set regulations on maximum contaminant level of nitrate at 44.28 and 50 mg/L, respectively [9,10]. Remediation technologies such as advanced biological nutrient treatment, electro-kinetic denitrification, reverse osmosis, and chemical reduction [11–15] have been developed to solve compelling issues of nitrate contamination in groundwater. However, these technologies are suffered from sludge generation [11], high operational cost [12–14], and undesirable by-product formation [15].

Catalytic reduction of nitrate to harmless nitrogen gas has captured an attention as a promising alternative for nitrate treatment since Vorlop and Tacke [16] demonstrated the effectiveness of bimetallic catalyst in 1989. Enormous efforts to find out the most effective metal combination in catalytic nitrate reduction have been made by loading Cu, Sn, Ni, Pd, Pt, Au, and Rh on diverse supporting materials [17–21] and Cu-Pd combination exhibited its high selectivity toward nitrogen gas production [21]. Since then, extensive studies have been focused on the determination of proper support material for Cu-Pd bimetallic catalyst to enhance catalytic denitrification because the performance of bimetallic catalyst is significantly influenced by properties of supports. Diverse support materials such as zero valent iron [17,21], silica-alumina [22], titania [23], activated carbon [18,24], alumina [25], and carbon nanotube [26] have been used for the bimetallic catalyst to improve its catalytic activity and selectivity in nitrate reduction. However, most of these studies on evaluation of efficient support materials have been conducted without any considerations of cost and toxicity of the support materials to date. Cost of carbon nanotube is relatively high [27], and application of nano-sized particles such as silica, titania, and carbon nanotube is still controversial due to their toxic effect on aquatic living life and even human health [28–30]. Therefore, a novel alternative support material needs to be developed to overcome these problems.

Maghemite (γ-$Fe^{III}_2O_3$), recently named as eco-nanomagnet [31], has been investigated due to its abundance and benign properties. The proven biocompatibility of maghemite has a promising potential to revolutionize its diverse applications from biomedicine and biosensor to in-situ remediation material [32] and can successfully solve toxicity issues caused by previously reported support materials. Another advantage of maghemite for a support material is its superparamagnetism which has been gradually in use

* Corresponding author. Tel.: +82 42 350 3624; fax: +82 42 350 3610.
E-mail address: woojin_lee@kaist.ac.kr (W. Lee).

0926-3373/$ – see front matter © 2012 Elsevier B.V. All rights reserved.
http://dx.doi.org/10.1016/j.apcatb.2012.08.017

and can provide more convenient, efficient, and less expensive way for collection of the magnetic particles, especially in high gradient magnetic separation [33]. Efficient collection of catalysts through magnetic field can prevent loss of deposited noble metals in the bimetallic catalyst system, ultimately lowering the reproduction cost of bimetallic catalyst. However, there is lack of knowledge on the evaluation of maghemite as a proper support material of bimetallic catalyst for effective and selective catalytic nitrate reduction. Thus, it is timely to develop a bimetallic catalyst supported by maghemite for the efficient, economical, and eco-friendly catalytic denitrification.

The objectives of this study were to develop a bimetallic catalyst supported by maghemite for catalytic nitrate reduction and to evaluate its stability and reusability. Thermal transformation of lepidocrocite was used to prepare maghemite. Cu and Pd were selected as a promoter and noble metal, respectively, and various contents of Cu and Pd were tested to improve catalytic activity and selectivity. The maghemite supported bimetallic catalyst (maghemite/Cu/Pd) was characterized by X-ray diffraction (XRD), temperature programmed reduction (TPR), scanning electron microscopy and energy dispersive X-ray (SEM/EDX), and transmission electron microscopy (TEM). X-ray photoelectron spectroscopy (XPS) analysis was conducted to investigate overall reaction mechanism for the nitrate reduction in this study.

2. Experimental

2.1. Chemicals

Lepidocrocite (γ-$Fe^{III}OOH$, Bayferrox 943) and hematite (α-$Fe^{III}_2O_3$, Bayferrox 105 M) were purchased from LANXESS Corp. Alumina (γ-Al_2O_3) was purchased from Sigma–Aldrich Inc. Precursor solutions of Cu and Pd were prepared with copper(II) chloride dihydrate (97.5%, Samchun Pure Chemical Co., Korea) and palladium(II) chloride (99.9%, Sigma–Aldrich Inc., USA), respectively. Sodium borohydride (98.0%, Samchun Pure Chemical Co., Korea) was used to reduce bimetallic catalyst. Potassium nitrite (97.0%, Samchun Pure Chemical Co., Korea), potassium nitrate (99.0%, Duksan Pure Chemical Co., Korea), and ammonium chloride (98.5%, Duksan Pure Chemical Co., Korea) were used for stock solution and standard solution for ion chromatography (IC) and Nessler method. Sodium bicarbonate (99.7%, Sigma–Aldrich Inc., USA) and sodium carbonate (99.95%, Sigma–Aldrich Inc., USA) were used to prepare eluent for IC operation. Deaerated deionized water (DDIW, 18 MΩ cm) was prepared with ultra pure water (ELGA PURELAB Classic system) by purging it with argon gas for 4 h. DDIW was stored in an anaerobic chamber filled with 95% Ar and 5% H_2 (Coy Laboratory Products Inc.).

2.2. Catalyst preparation

In this study, nano-sized maghemite was prepared as a support for bimetallic catalyst. Thermal transformation of lepidocrocite was performed to prepare maghemite having higher surface area than magnetite-derived maghemite [34]. The bimetallic catalyst was prepared through impregnation method [35]. Lepidocrocite (1.44 g) mixed with DDIW (200 mL) was undergone ultrasonic vibration for 10 min before addition of precursors. Concentrations of each precursor solution were adjusted to produce targeted from 0.25 to 1 wt.%. Lepidocrocite suspension was successively mixed with prepared Cu and Pd precursors under continuous stirring (100 rpm) at room temperature (25 ± 0.5 °C) for 2 h each. Mixed solution of lepidocrocite with Cu and Pd precursors was dried in an oven at 100 °C for 24 h for complete removal of water. Dried catalyst was calcinated at 350 °C for 2 h to transform lepidocrocite to maghemite and to coat Cu and Pd on the surface. Orange color of lepidocrocite turned into brown color of maghemite via calcination. Maghemite containing Cu and Pd was reduced by dropwise addition of $NaBH_4$ (0.01 mM) solution according to the following reaction [25]:

$$2Cu^{2+} + BH_4^- + 3H_2O \rightarrow 2Cu(0) + B(OH)_3 + 2H_2 + 3H^+ \quad (1)$$

$$2Pd^{2+} + BH_4^- + 3H_2O \rightarrow 2Pd(0) + B(OH)_3 + 2H_2 + 3H^+ \quad (2)$$

Bivalent Cu and Pd ions on the support surface reduced to zero-valent solid phases (Eqs. (1) and (2)). Maghemite/Cu/Pd was vacuum-filtered with 0.2 μm mixed cellulose ester membrane filter (Adventac) and washed with DDIW twice to remove residual chemicals. Washed bimetallic catalyst was sonificated for 5 min for complete dispersion of particle and immediately used for a batch experiment. No loss of metal during each preparation step was alumina/Cu/Pd and hematite/Cu/Pd catalysts were prepared via identical methods described above.

2.3. Experimental procedures

The catalytic nitrate reduction tests were conducted in a 500 mL glass batch reactor equipped with a mechanical stirrer, a H_2 gas supply inlet, a gas outlet, a sampling port, and an injection port. The gas outlet was connected with ammonia capturing container filled with 100 mL of H_2SO_4 (10%, v/v) to collect stripped ammonia gas during nitrate reduction. 199.7 mL of DDIW (pH 5.7) containing maghemite/Cu/Pd (0.16 g) was filled in the reactor and continuously stirred with a mechanical stirrer. 0.3 mL of nitrate stock solution (88,560 mg/L) was injected through the injection port to provide an initial concentration of 132.8 mg/L. The reaction was initiated after nitrate injection under continuous stirring (100 rpm) with a mechanical stirrer at room temperature. Hydrogen gas was continuously introduced into the batch reactor through the diffuser during the reaction to provide bimetallic catalyst with hydrogen and keep an anaerobic condition.

Nitrate removal by maghemite/Cu/Pd was compared with that by two different catalysts and control (alumina/Cu/Pd, hematite/Cu/Pd, and maghemite only) to investigate the role of maghemite as a supporting material for bimetallic catalyst. Unless stated otherwise, loading of Cu and Pd were fixed at 0.5 wt.% each, and hydrogen gas flow rate was fixed at 100 cc/min. Batch experiments were conducted to investigate the effect of metal (Cu and Pd) loading and hydrogen gas flow rate on nitrate removal and selectivity of by-product. To investigate the effect of metal loading, we used four different levels of Cu loading (0.25, 0.5, 0.75, and 1 wt.%) with 0.5 wt.% of Pd and four different levels of Pd loading (0.25, 0.5, 0.75, and 1 wt.%) with 0.5 wt.% of Cu. Loading of Cu and Pd was confirmed by inductively coupled plasma mass spectrometer (ICP-MS, Optima 7300 DV, PerkinElmer). The effect of hydrogen gas flow rate was investigated at five different flow rates of hydrogen gas (100, 200, 300, 400, and 500 cc/min). Nitrate removal and selectivity by maghemite/Cu/Pd during three reaction cycles were also investigated to evaluate reusability of maghemite/Cu/Pd. For regeneration of the catalysts, maghemite/Cu/Pd was collected by magnetic bar after each reaction cycle and vacuum-filtered to minimize loss of catalysts. Collected maghemite/Cu/Pd were washed with DDIW to remove residual ions on the surface, dried at 100 °C for 24 h, calcinated at 350 °C, and reduced by $NaBH_4$ as described above. In order to compensate the loss of catalyst, the volume of DDIW was adjusted to fix the same concentration of catalyst for second and third cycles. Also initial amount of nitrate was adjusted to remain the same initial nitrate concentration (132.8 mg/L).

2.4. Analytical procedures

Concentrations of nitrate and nitrite were measured by using IC (DX-120, Dionex Co.) equipped with Dionex IonPac AS 14 column (4 mm × 250 mm), conductivity detector, and Dionex AS40 autosampler. Mixture of Na_2CO_3 (3.5 mM) and $NaHCO_3$ (3.5 mM) was prepared for IC eluent. 5 mL of samples were taken out from the batch reactor through 5 mL-disposable syringe (Korea Vaccine Corp.), and the sample was immediately filtered with 0.2 μm mixed cellulose ester membrane filter. 4 mL of the filtrate was analyzed to measure concentrations of nitrate and nitrite through IC.

Colorimetric measurement of ammonium was conducted using a spectrophotometer (DR-2010, HACH) at 415 nm using Nessler method. 1 mL of the remained filtrate after IC analysis was used to measure concentration of ammonium through Nessler method. At the same sampling time, 1 mL of H_2SO_4 was also collected from the ammonia capturing container to measure concentration of stripped ammonia because captured ammonia in H_2SO_4 was dissolved and transformed to ammonium ion [15]. Total ammonium concentration produced during at each sampling time was the sum of ammonia concentrations from the batch reactor and ammonia capturing container, respectively.

The removal of nitrate ($R_{NO_3^-}$) and selectivity of each by-product ($S_{\text{by-product}}$) were calculated as followed:

$$R_{NO_3^-}(\%) = \frac{[NO_3^-]_i - [NO_3^-]_f}{[NO_3^-]} \quad (3)$$

$$S_{NO_2^-}(\%) = \frac{[NO_2^-]_f}{[NO_3^-]_i - [NO_3^-]_f} \quad (4)$$

$$S_{NH_3^+}(\%) = \frac{[NH_3^+]_f}{[NO_3^-]_i - [NO_3^-]_f} \quad (5)$$

$$S_{N_2}(\%) = \frac{[NO_3^-]_i - [NO_3^-]_f - [NO_2^-]_f - [NH_4^+]_f}{[NO_3^-]_i - [NO_3^-]_f} \quad (6)$$

where subscriptions of i and f refer to initial and final stage of reaction, respectively. Selectivity toward nitrogen gas was calculated by difference in nitrogen mass balance (Eq. (6)) assuming that production of NO_x and N_2O gases was negligible [21,26,36].

Surface area of lepidocrocite, maghemite, and maghemite/Cu/Pd was measured to investigate their changes after calcination and metal deposition. After preparing each material, they were dried in anaerobic chamber for 24 h. Specific surface areas of samples were measured by nitrogen adsorption and desorption at −196 °C with BET surface analyzer (ASAP 2010, Micrometrics).

Lepidocrocite, maghemite, and maghemite/Cu/Pd were identified by XRD using Rigaku automated diffractometer with Cu KN radiation (D/MAX-RB, Rigaku). Dried samples prepared by following the sample preparation procedure of BET analysis were carefully transferred to XRD template in the anaerobic chamber to avoid oxidation of the samples. The samples were scanned between 10° and 70° at a scan speed of 2° min^{-1}. Beam voltage and current were 40 kV and 300 mA, respectively. The identity of samples was checked by analyzing their XRD patterns with Joint Committee on Powder Diffraction Standards (JCPDS) diffraction data files (JADE 9, Materials Data, Inc.).

Distribution of Cu and Pd particles was investigated via TPR experiment. Maghemite/Cu/Pd (0.1 g) without $NaBH_4$ treatment was introduced into a conventional flow system for the TPR analysis (Catalyst analyzer, Belcat) and examined in the temperature range of 50–600 °C with ramping of 5 °C/min. 5% H_2/Ar was passed through the system bed at flow rate of 30 cc/min. hematite/Cu/Pd and alumina/Cu/Pd were undergone the same procedure as controls for the TPR analysis.

Table 1
BET surface area of lepidocrocite, maghemite, and maghemite/Cu/Pd (0.5 wt.% of Cu and Pd).

Material	BET surface area (m^2 g−1)
Lepidocrocite	75
Maghemite	21
Maghemite/Cu/Pd	24

Dispersion of Cu and Pd particles on the surface of maghemite was identified by SEM/EDX (Sirion, FEI). EDX mapping was performed to visualize elemental and spatial information of Cu, Pd, and Fe on the maghemite surface. The same sample preparation procedure for the BET analysis was used for the preparation of samples (maghemite/Cu/Pd and lepidocrocite) for the SEM/EDX analysis. Dried samples were carefully transferred to carbon tape on SEM template in the anaerobic chamber to avoid oxidation of the samples. They were coated by osmium coater and analyzed by SEM at 10 kV. The morphology of maghemite/Cu/Pd was characterized by TEM (JEM-3010 model, JEOL). Maghemite/Cu/Pd was diluted with ethanol [37] and underwent sonication for 10 min to disperse aggregated maghemite particles. Several drops of the diluted sample were put on 300-mesh gold TEM grid with a carbon film and the grid was dried in the anaerobic chamber for 1 h. Samples were analyzed by TEM at 300 kV.

Measurements of Cu and Pd during each recycling test were conducted to confirm if leaching of Cu and Pd occurred during the reaction. 20 mL of sample was taken out from the reactor and vacuum-filtered with 0.2 μm mixed cellulose ester membrane filter. Cu and Pd leached from the maghemite/Cu/Pd surface were identified and quantified with ICP-MS.

XPS analysis (MultiLab 2000, Thermo) was carried out to investigate the oxidation state of surface Fe for differentiating maghemite from magnetite and to check changes of oxidation state of Cu and Pd on the surface of maghemite/Cu/Pd before and after catalytic nitrate reduction. Maghemite/Cu/Pd was collected by vacuum-filtering the catalyst suspension with 0.2 μm mixed cellulose ester membrane filter after the reaction and washed with DDIW twice, followed by ethanol. Maghemite/Cu/Pd was dried and kept in the anaerobic chamber until XPS analysis. Dried samples (maghemite/Cu/Pd before and after the reaction) were carefully packed on XPS sampling template in the anaerobic chamber to avoid oxidation of each sample. Adjustment from surface charging effects was made with C1S peak at 285 eV as a reference peak, and Shirley baseline and a Gaussian–Lorentzian peak shape were used for data fitting.

3. Results and discussion

3.1. Catalyst characterization

Specific surface areas of lepidocrocite, maghemite, and maghemite/Cu/Pd were measured to investigate the effect of calcination and metal addition on the change of surface area (Table 1). Surface area of lepidocrocite decreased from 75 to 21 m^2 g^{-1} via thermal transformation to maghemite. This is due to condensation of lepidocrocite surface through endothermic abstraction of water during thermal treatment at 350 °C [38]. Addition of Cu (0.5 wt.%) and Pd (0.5 wt.%) to maghemite did not significantly change the surface area of maghemite/Cu/Pd (21–24 m^2 g^{-1}) due to low concentrations (0.5 wt.%) of Cu and Pd deposited on the maghemite surface.

XRD analysis was conducted to identify lepidocrocite, maghemite, and maghemite/Cu/Pd. Fig. 1(a) shows narrow and well-ordered peaks of initial pure lepidocrocite. After calcination of the lepidocrocite at 350 °C, its peaks disappeared and new peaks corresponding to the standard peaks of maghemite (Fig. 1(b))

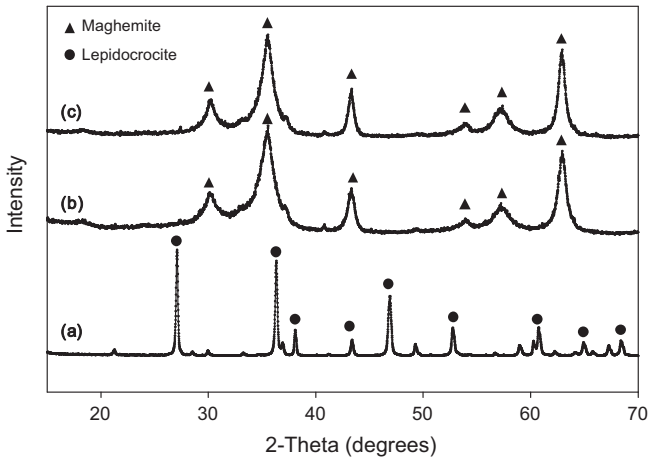

Fig. 1. XRD patterns of (a) lepidocrocite, (b) maghemite, and (c) maghemite/Cu/Pd (0.5 wt.% of Cu and Pd): peaks of lepidocrocite (●) and peaks of maghemite (▲).

appeared indicating that lepidocrocite was thermally transformed to maghemite at 350 °C. XRD pattern of maghemite/Cu/Pd shown in Fig. 1(c) is very similar to that of maghemite. Cu(0) and Pd(0) peaks were not detected in the XRD diffractogram of maghemite/Cu/Pd because amount of each metal addition was not high enough to detect the peaks by XRD analysis. Differentiation of maghemite from magnetite ($Fe^{II}{}_1{}^{III}{}_2O_4$) by XRD analysis is very difficult due to their similar crystal structure [39], therefore, XPS analysis was performed in the range of 700–720 eV [40] to investigate the oxidation states of Fe on maghemite/Cu/Pd surface (Fig. 2). Narrow scan of Fe(2p) was composed of only a clear peak of Fe(III) at 712 eV, while peak of Fe(II) at 709–709.5 was not observed by XPS analysis. XPS results show that reduced phases of Fe (i.e., Fe(II) or Fe(0)) did not form on maghemite/Cu/Pd surface after reduction with $NaBH_4$ but existed only Fe(III) specie confirming that only maghemite formed during the synthesis of maghemite/Cu/Pd.

TPR analysis was carried out for investigation of Pd and Cu distribution (Fig. 3). In all cases, there was no peak around 60 °C which attributes to the decomposition of Pd β-hydride, indicating wide dispersion of Pd particles [26,41]. TPR profile of maghemite/Cu/Pd (Fig. 3(a)) shows one sharp peak centered at 90 °C. H_2 consumption at 90 °C was 121 μmol g^{-1}, which is very near the sum of theoretical H_2 consumption for reduction of Pd (0.5 wt.%, 47 μmol g^{-1}) and Cu (0.5 wt.%, 79 μmol g^{-1}) species. This indicates that the peak at 90 °C should be ascribed to co-reduction of the Pd and Cu

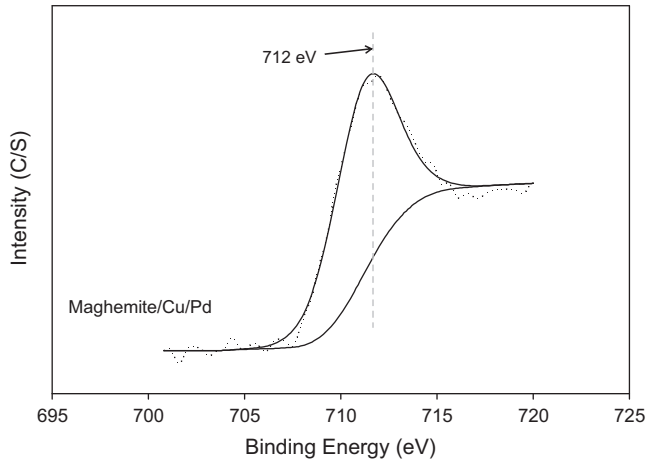

Fig. 2. XPS spectra for the narrow scan of Fe(2p) on the surfaces of maghemite/Cu/Pd (0.5 wt.% of Cu and Pd).

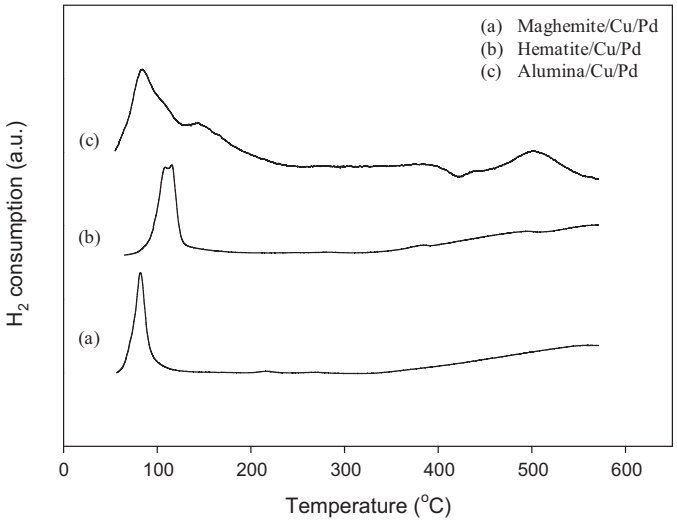

Fig. 3. TPR profile for (a) maghemite/Cu/Pd, (b) hematite/Cu/Pd, and (c) alumina/Cu/Pd. For all bimetallic catalysts, 0.5 wt.% of Cu and Pd were deposited.

species due to the reduction of Cu oxide promoted by hydrogen spillover from Pd [42]. TPR profile of maghemite/Cu/Pd also shows broad increase in H_2 consumption starting around 350 °C. It has been reported that $Fe^{III}{}_2O_3$ is transformed to magnetite around 400 °C via thermal reduction with H_2 during TPR analysis [43,44]. However, the increase in H_2 consumption was detected at temperature lower than 400 °C because Pd enhanced the reduction of maghemite to magnetite [45]. Similar pattern of TPR profile, one sharp peak and broad increase, was obtained with hematite/Cu/Pd (Fig. 3(b)). However, the sharp peak was shifted to higher temperature (120 °C) than that of maghemite/Cu/Pd. This indicates that maghemite/Cu/Pd has closer contact between Cu and Pd for hydrogen spillover compared with hematite/Cu/Pd [45]. The broad increase in H_2 consumption around 350 °C in TPR profile of hematite/Cu/Pd showed transformation to magnetite during TPR analysis, which was also observed in the case of maghemite/Cu/Pd [44]. TPR profile of alumina/Cu/Pd shows one peak around 90 °C (Fig. 3(c)). This is due to reduction of Cu oxide by spillover of hydrogen via Pd as similarly observed in maghemite/Cu/Pd and hematite/Cu/Pd [42].

SEM/EDX analysis was performed to investigate morphological characteristics of lepidocrocite and maghemite/Cu/Pd (Figs. 4 and 5). Fig. 4(a) shows rectangular and platy shape particles with a size of 50–200 nm which has been identified as lepidocrocite [46]. The shape and size of maghemite/Cu/Pd (Fig. 4(b)) was similar to those of lepidocrocite. It has been reported that maghemite derived from mother material follows morphological properties of mother material [34,39]. Therefore, the shape and size of maghemite/Cu/Pd did not significantly change from those of lepidocrocite. EDX mapping was carried out to investigate elemental constituents and distribution pattern of Cu and Pd on the surface of maghemite (Fig. 5). Fig. 5(a) shows the image of maghemite/Cu/Pd which was analyzed for the EDX mapping. Fe was ubiquitously detected (Fig. 5(b)) because maghemite mainly consists of Fe(III). Cu was sparsely found on the maghemite surface and its distribution pattern was fairly uniform (Fig. 5(c)), while Pd was more densely deposited and well-dispersed on the maghemite surface (Fig. 5(d)). This is because the successive addition of Pd after Cu may have covered Cu deposited on the maghemite surface resulting in more exposure of Pd on the surface [21].

TEM analysis was conducted to investigate morphological characteristics of maghemite/Cu/Pd in detail (Fig. 6). Similar rectangular and platy shape of maghemite particles (50–200 nm; Fig. 6(a))

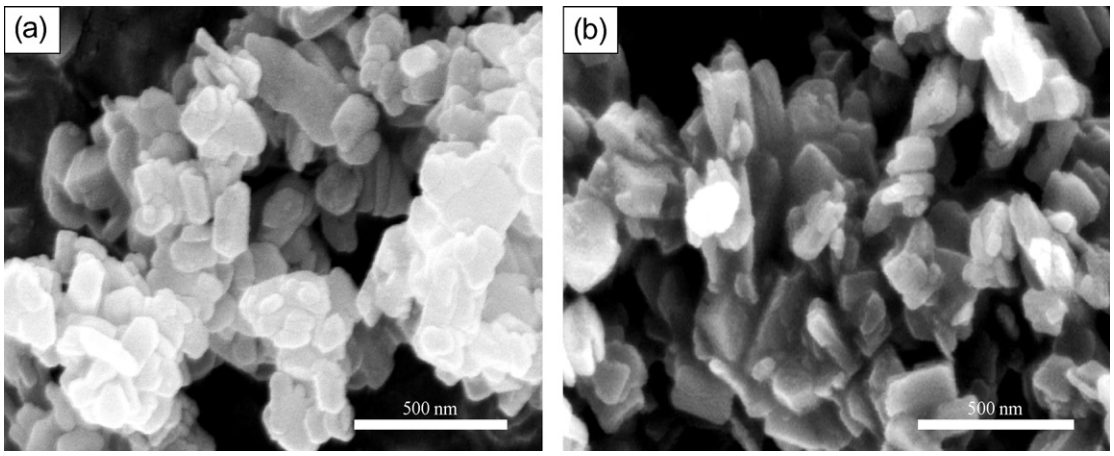

Fig. 4. SEM images of (a) lepidocrocite and (b) maghemite/Cu/Pd (0.5 wt.% of Cu and Pd).

were also observed as shown by SEM analysis above (Fig. 5(a)). Maghemite deposited with Cu (0.5 wt.%) and Pd (0.5 wt.%) demonstrated that tiny particles (1–5 nm, Fig. 7(a)) were uniformly scattered on the maghemite surface (Fig. 6(c)). EDX analysis revealed that those particles are Cu and Pd particles (Fig. 6(d)), which is consistent to the results from amorphous silica-alumina [22], titania [23], and activated carbon [24] supports. The TEM images show that Cu and Pd particles on the maghemite surface are 10–200 times smaller than maghemite. Bimetal particles of which size are below 10 nm have been considered as potentially well and densely distributed particles compared to unevenly aggregated particles [23]. Maghemite provided a suitable surface environment for the dense and uniform deposition of Cu and Pd particles, which is a significant key factor to determine catalytic activity of catalysts [22]. Fig. 6(e and f) showed maghemite/Cu/Pd with different metal loading at 1/0.5 wt.% and 0.5/1 wt.% of Cu/Pd, respectively. Particle size distributions of maghemite/Cu/Pd (1/0.5 wt.%) and maghemite/Cu/Pd (0.5/0.1 wt.%) are similar to that of maghemite/Cu/Pd (0.5/0.5 wt.%) (Fig. 7(a–c)). This indicates that increased amount of bimetal loading from 0.5 to 1 wt.% did not significantly change particle size distribution in this study.

3.2. Catalytic nitrate reduction by maghemite/Cu/Pd

3.2.1. Nitrate reduction by maghemite/Cu/Pd

Fig. 8 shows the catalytic nitrate reduction by maghemite, maghemite/Cu/Pd, alumina/Cu/Pd, and hematite/Cu/Pd. Nitrate reduction by maghemite without Cu and Pd was not significant

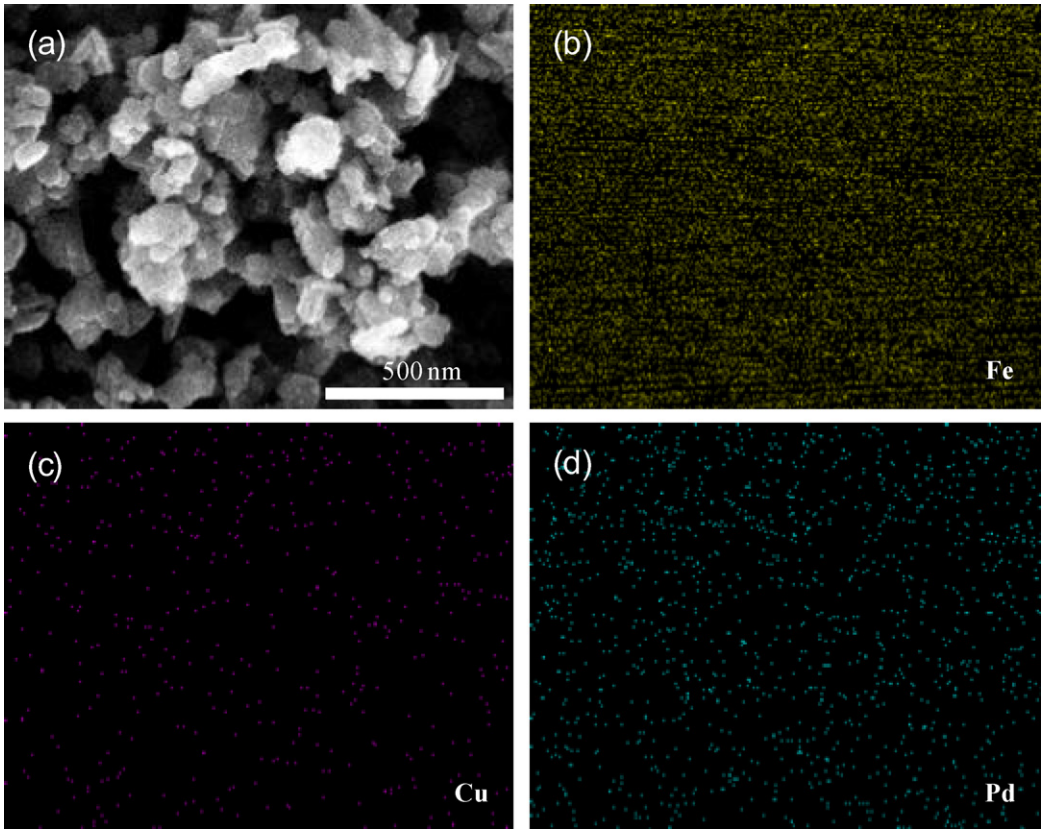

Fig. 5. SEM/EDX images of (a) maghemite/Cu/Pd (0.5 wt.% of Cu and Pd), (b) Iron Ka1, (c) Cu Ka1, and (d) Pd La1.

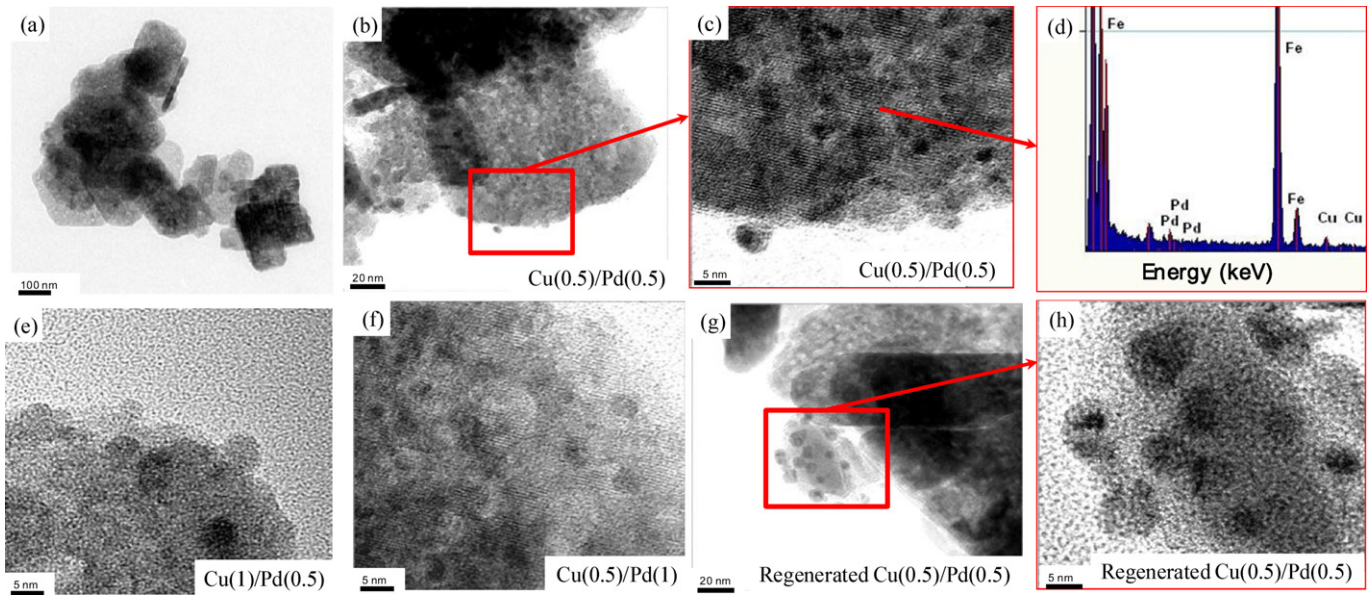

Fig. 6. TEM images of (a) Maghemite, (b) maghemite/Cu/Pd (0.5 wt.% of Cu and Pd), (c) magnified version of maghemite/Cu/Pd (0.5 wt.% of Cu and Pd), (d) EDX spectra of maghemite/Cu/Pd (0.5 wt.% of Cu and Pd), (e) maghemite/Cu/Pd (1/0.5 wt.% of Cu/Pd), (f) maghemite/Cu/Pd (0.5/1 wt.% of Cu/Pd), (g) regenerated maghemite/Cu/Pd (0.5 wt.% of Cu and Pd), and (h) magnified version of regenerated maghemite/Cu/Pd (0.5 wt.% of Cu and Pd).

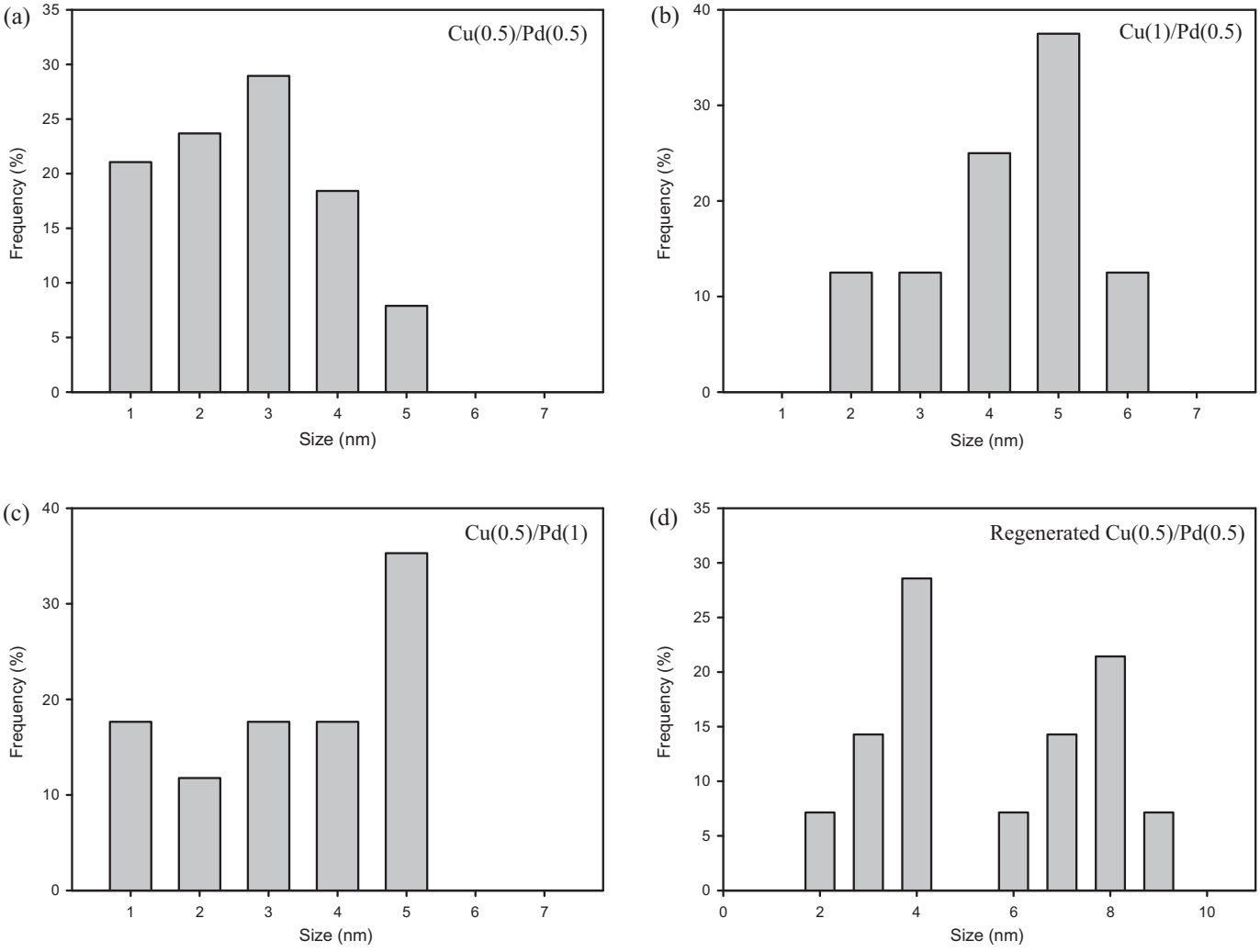

Fig. 7. Particle size distribution of (a) maghemite/Cu/Pd (0.5 wt.% of Cu and Pd), (b) maghemite/Cu/Pd (1/0.5 wt.% of Cu/Pd), (c) maghemite/Cu/Pd (0.5/1 wt.% of Cu/Pd), and (d) regenerated maghemite/Cu/Pd (0.5 wt.% of Cu and Pd).

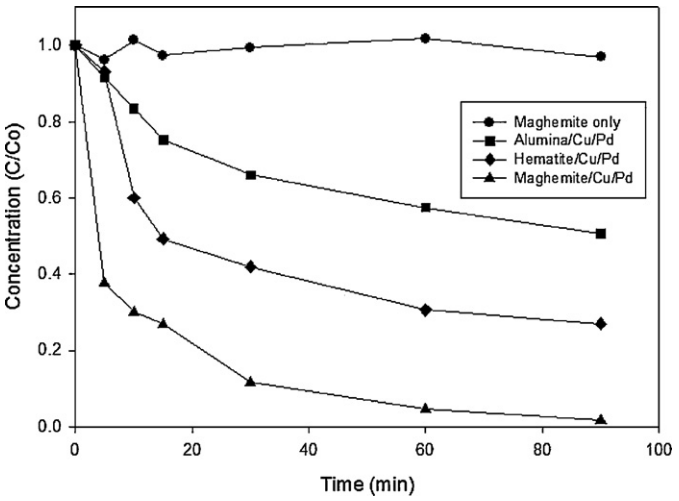

Fig. 8. Catalytic nitrate reduction by different bimetallic catalysts (0.8 g/L) with hydrogen flow (100 cc/min): (a) maghemite only (●), (b) alumina/Cu/Pd (■), (c) hematite/Cu/Pd (♦), and (d) maghemite/Cu/Pd (▲). For (b–d), 0.5 wt.% of Cu and Pd were deposited. Reaction time was 90 min.

(only 3% removal efficiency) showing that role of Fe can be negligible in this study. Moreover, we confirmed that there was no Fe(II) and Fe(0) species on the catalyst surface via XPS analysis (Fig. 2). To date, most of the studies dealing with nitrate reduction with iron oxide have used ferrous oxides and zero valent iron (or nano-zero valent iron) which work as electron donors [15,47,48]. However, in this research, maghemite is one of ferric oxides, which does not possess electron donating capability. Complete nitrate removal (99.5%) was observed by maghemite/Cu/Pd at 90 min, while hematite/Cu/Pd showed 63% removal. This is due to higher surface area of maghemite/Cu/Pd (24 $m^2 g^{-1}$) than that of hematite/Cu/Pd (3 $m^2 g^{-1}$) (Table 2). Generally, high surface area of supporting material can provide more active sites for catalytic nitrate reduction [23,49]. However, alumina/Cu/Pd showed a contradictory result. alumina/Cu/Pd has a significantly higher surface area (186 $m^2 g^{-1}$) than that of maghemite/Cu/Pd (24 $m^2 g^{-1}$) but nitrate removal by alumina/Cu/Pd (43%) was much lower than that of maghemite/Cu/Pd (99.5%). This is due to the difference in pore volume of support material, i.e. the pore volume of alumina/Cu/Pd (0.408 $cm^3 g^{-1}$) is approximately 5 times higher than that of maghemite/Cu/Pd (0.079 $cm^3 g^{-1}$) and hematite/Cu/Pd (0.069 $cm^3 g^{-1}$). Because hydroxide ions formed through hydrogenation of oxygen molecule in nitrite structure during the catalytic nitrate reduction, they could be trapped in pores of support materials resulting in accumulation of hydroxide ions in the pores [42]. Accumulated hydroxide ions leading to their adsorption on the active sites of Cu and Pd may inhibit catalytic activity of the bimetals [5,20]. This explains that the higher pore volume of alumina/Cu/Pd with more accumulated hydroxide ions negatively influences the catalytic nitrate reduction.

Table 2
BET surface area and pore size of alumina/Cu/Pd, maghemite/Cu/Pd, and hematite/Cu/Pd (0.5 wt.% of Cu and Pd).

Material	BET surface area ($m^2 g^{-1}$)	Pore volume ($cm^3 g^{-1}$)
Alumia/Cu/Pd	186	0.408
Maghemite/Cu/Pd	24	0.079
Hematite/Cu/Pd	3	0.069

3.2.2. Effect of Cu loading variation on nitrate reduction and selectivity

Fig. 9 shows the nitrate removal and selectivity by maghemite/Cu/Pd at four different levels of Cu loading. All experimental cases showed high removal of nitrate (>95%). A volcano shaped pattern was observed for nitrogen gas selectivity as Cu loading increased. The highest nitrogen gas selectivity (43%) was found at 0.5 wt.% of Cu loading, and the other cases were below 25%. Catalytic nitrate reduction can be explained with two successive reactions induced by Cu and Pd. Nitrate is firstly adsorbed on the Cu surface and reduced to nitrite [21], and subsequently reduced to ammonium or nitrogen gas by hydrogen molecules adsorbed on active sites of Pd surface [23,45]. Therefore, proximity between Cu and Pd particles is a significant factor to determine catalytic activity in nitrate reduction. Our results indicate that the proximity between Cu and Pd particles at 0.5/0.5 wt.% of Cu/Pd was optimal to produce maximum amount of nitrogen gas. Nitrite selectivity increased from 9.7 to 42.4% as Cu loading increased, while ammonium selectivity decreased from 64.3 to 42%. Increase in Cu content (0.25–1 wt.%) reduced more nitrate to nitrite, while further reduction of nitrite cannot be enhanced due to fixed amount of Pd (0.5 wt.%). Therefore, more nitrite was accumulated resulting in higher selectivity of nitrite.

3.2.3. Effect of Pd loading on nitrate reduction and selectivity

Fig. 10 shows the nitrate removal and selectivity by maghemite/Cu/Pd with four different levels of Pd loading. In all experimental cases, nitrate removal was higher than 95% and nitrite selectivity was significantly low (<12%) compared to nitrogen gas and ammonium selectivities. These results indicate that both nitrate and nitrite reductions were successfully achieved during the entire Pd loading experiments. The nitrogen gas selectivity decreased from 47 to 22% as Pd loading increased, while its selectivity for ammonium dramatically increased from 40 to 75%. It has been known that nitrogen gas forms via recombination of nitrogen atoms by activated hydrogen molecules adsorbed on the active sites of Pd particles [21,48]. The hydrogen molecules can abstract oxygen molecules from nitrite, and two nitrogen atoms are consecutively bonded to form the nitrogen gas [18,50]. However, our experimental results showed a different pattern of nitrogen atom recombination due to excessive amount of hydrogen molecules at the active sites of Pd, as Pd loading increased. After the abstraction of oxygen molecules, nitrogen atoms were bonded with an excessive amount of accumulated hydrogen molecules leading to the formation of ammonium rather than that of nitrogen gas [25]. The results suggest that excessive Pd loadings on maghemite/Cu/Pd surface can cause an inhibitive effect on the reductive transformation of nitrogen gas from nitrite.

3.2.4. Effect of H_2 flow rate on nitrate reduction and selectivity

Fig. 11 shows nitrate removal and selectivity by maghemite/Cu/Pd at five different hydrogen flow rates. Nitrate removal was higher than 94% in all cases and nitrite selectivity was significantly low (<12%) compared to nitrogen gas and ammonium selectivities. These results confirm excellent catalytic activity of maghemite/Cu/Pd to reduce nitrate and nitrite under all different hydrogen flow rates. Selectivities of nitrogen gas at low flow rates (100 and 200 cc/min) were slightly higher (43 and 45%) than those at high flow rates (>300 cc/min; 28%). On the other hand, selectivity of ammonium increased from 54.6 to 67.5% as flow rate of hydrogen increased, which is consistent to the results obtained from the Pd loading experiment. As mentioned above, the formation of ammonium is significantly dependent on the accumulation of hydrogen molecules on active sites of Pd [50]. High content of hydrogen molecules may accumulated on the active

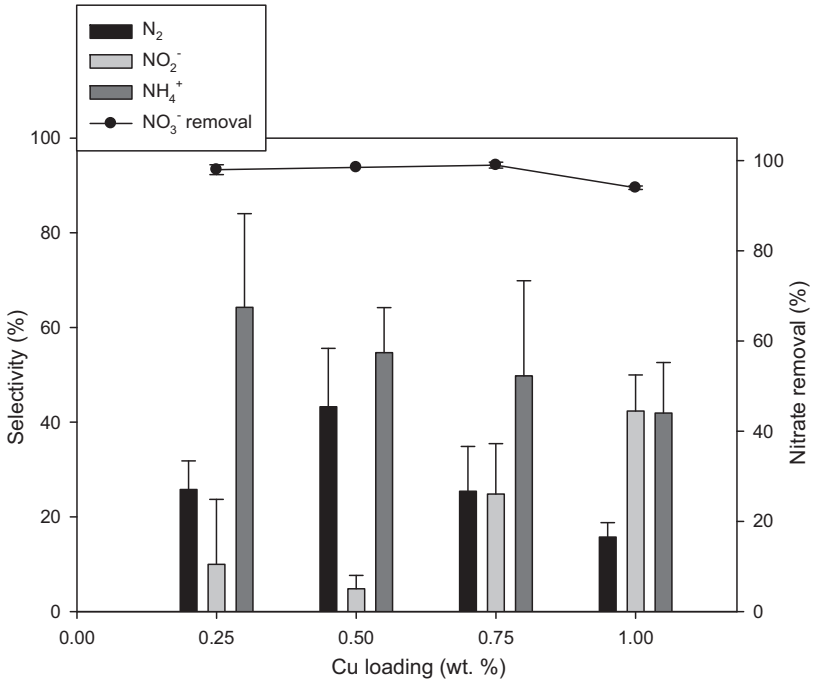

Fig. 9. By-product selectivity and nitrate removal (●) by different Cu loadings on maghemite/Cu/Pd (0.8 g/L) with hydrogen flow rate (100 cc/min): Cu loadings were 0.25, 0.5, 0.75, and 1 wt.%: Pd loading was fixed at 0.5 wt.%. Reaction time was 90 min. Error bars demonstrate standard deviation of duplicate experiments.

sites of Pd as hydrogen flow rate increased, resulting in promoting the formation of ammonium rather than that of nitrogen gas. Therefore, the formation of nitrogen gas in the catalytic nitrate reduction by maghemite/Cu/Pd was also inhibitively influenced by the increase of hydrogen flow rate.

3.3. Recycling of maghemite/Cu/Pd for catalytic nitrate reduction

Fig. 12 shows the nitrate removal and selectivity by maghemite/Cu/Pd during three reaction cycles. maghemite/Cu/Pd completely reduced nitrate (99.5%) at first cycle, while its removal

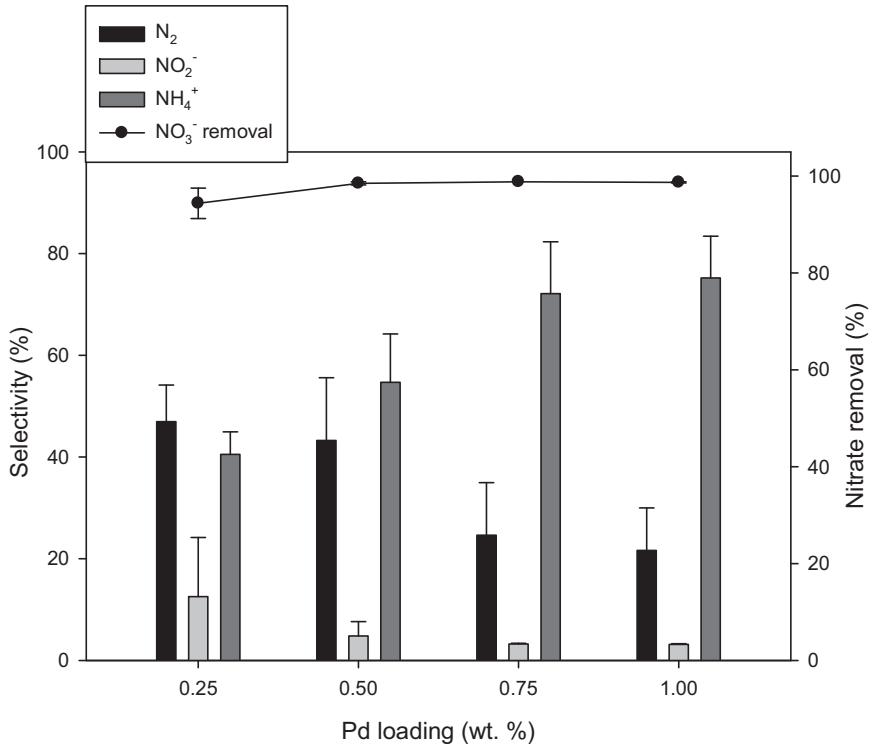

Fig. 10. By-product selectivity and nitrate removal (●) by different Pd loadings on maghemite/Cu/Pd (0.8 g/L) with hydrogen flow rate (100 cc/min): Pd loadings were 0.25, 0.5, 0.75, and 1 wt.%: Cu loading was fixed at 0.5 wt.%. Reaction time was 90 min. Error bars demonstrate standard deviation of duplicate experiments.

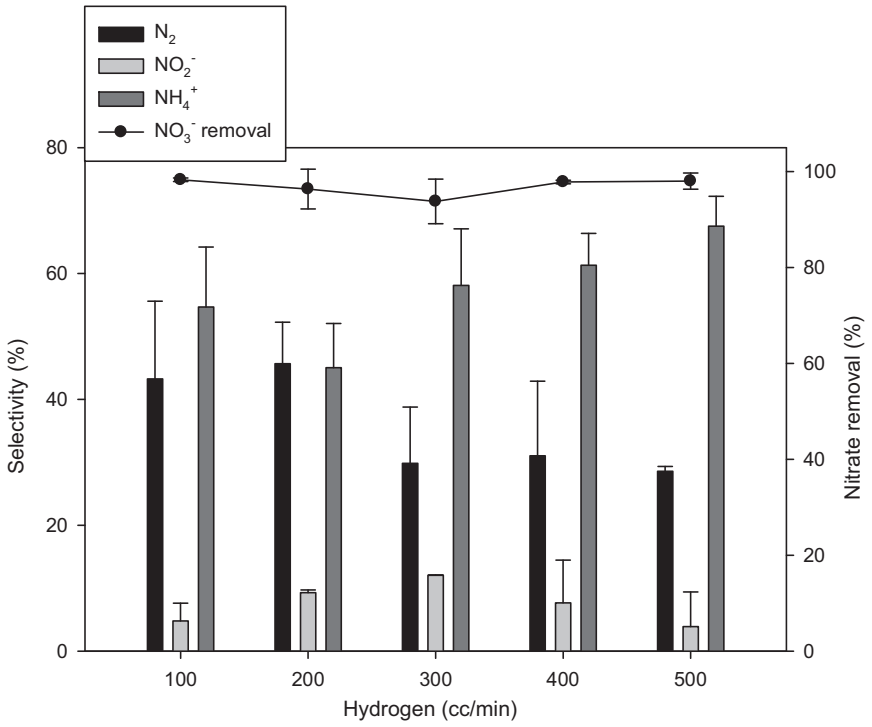

Fig. 11. By-product selectivity and nitrate removal (●) by maghemite/Cu/Pd (0.5 wt.% of Cu and Pd, 0.8 g/L) under different hydrogen flow rates: hydrogen flow rates were 100, 200, 300, 400, and 500 cc/min. Reaction time was 90 min. Error bars demonstrate standard deviation of duplicate experiments.

decreased to 85.5% and 83% at second and third cycle, respectively. This is due to loss of active sites of Cu through sintering of Cu particles after first regeneration procedure. The size of regenerated particles (Figs. 6(h) and 7(d)) significantly increased via sintering comparing with fresh maghemite/Cu/Pd (Figs. 6(c) and 7(a)). It has been previously reported that the particle size of Cu on Cu/ZnO [51], Cu/ZnO/Al_2O_3 [52], and CuO/SiO_2 [53] also increased during the regeneration step. However, maghemite/Cu/Pd exhibited more excellent removal and stability in recycle of catalyst than titania/Pt/Re [54], silica-alumina/Cu/Pd, and alumina/Cu/Pd [22]. The results confirm that maghemite/Cu/Pd was an efficient and durable catalyst for the recycle for the catalytic nitrate reduction. The selectivity of nitrogen gas slightly decreased at second cycle (26%) and increased at third cycle (31%). The average value

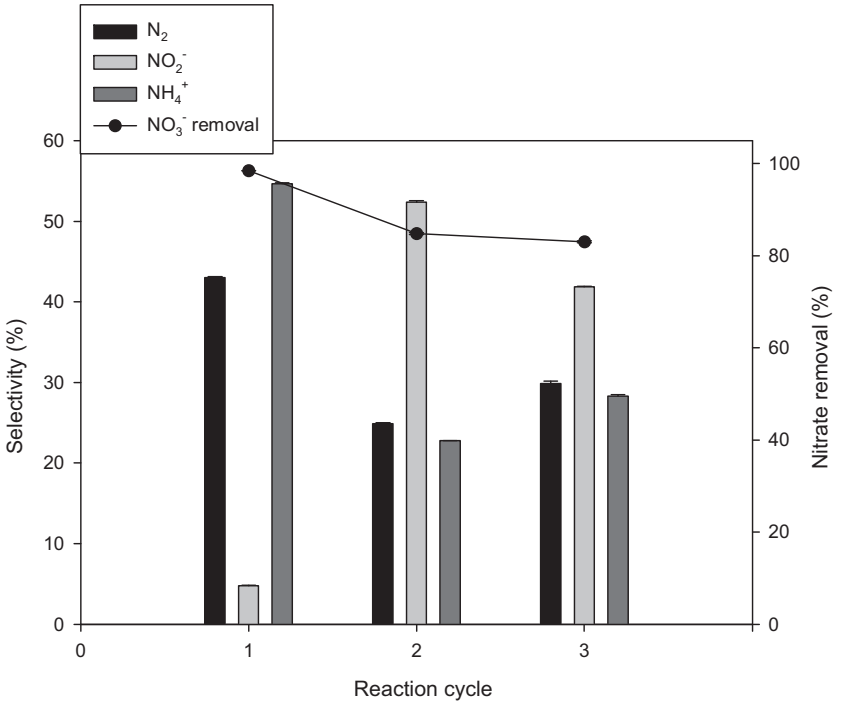

Fig. 12. By-product selectivity and nitrate removal (●) by maghemite/Cu/Pd (0.5 wt.% of Cu and Pd, 0.8 g/L) at hydrogen flow rate (100 cc/min) during three reaction cycles. Reaction time was 90 min. Error bars demonstrate standard deviation of duplicate experiments.

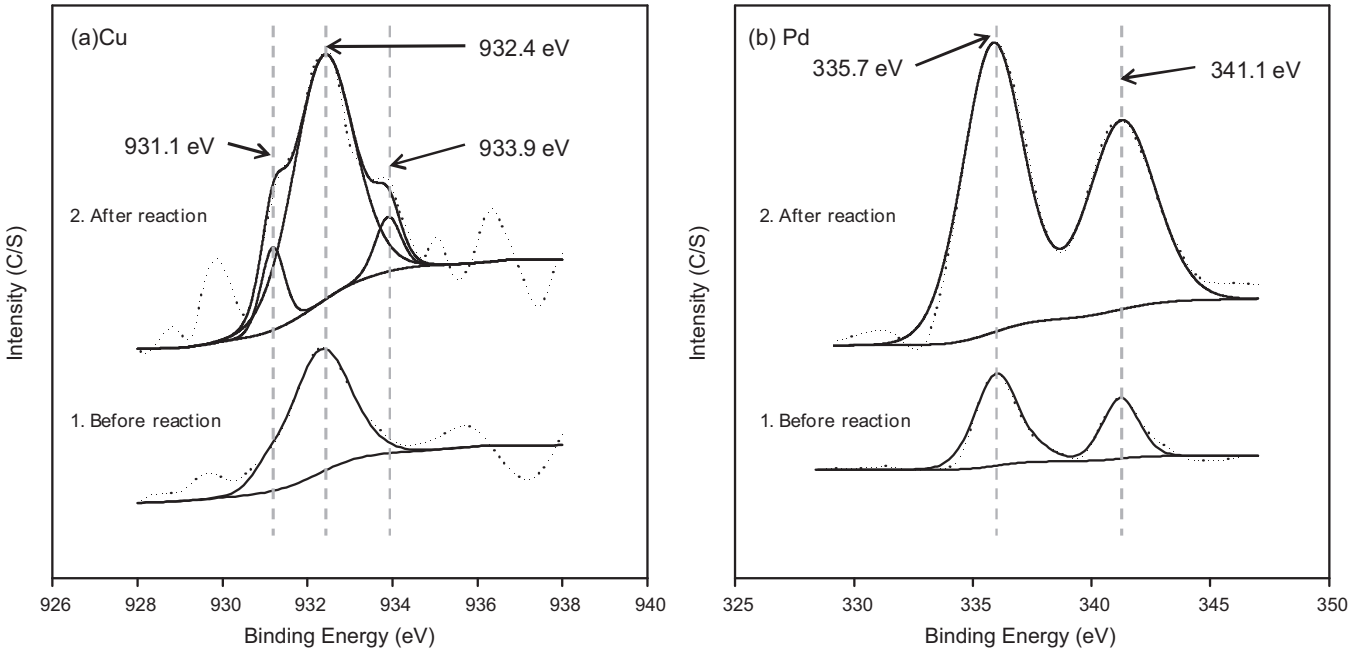

Fig. 13. XPS spectra for the narrow scan of (a) Cu(2p) and (b) Pd(3d) on the surface of maghemite/Cu/Pd before (1) and after (2) reaction (0.5 wt.% of Cu and Pd).

throughout three cycles was higher than 30% showing a stable selectivity of maghemite/Cu/Pd for the catalytic reduction of nitrate to nitrogen gas. However, nitrite selectivity dramatically increased from 5 to 53% after first cycle and reached relatively constant value (43%) at third cycle. This occurred due to the aggregation of Pd particles during the recycling tests (Figs. 6(f) and 7(d)). It has been reported that Pd particles aggregated each other during the catalytic nitrate reduction [22]. The aggregated Pd particles easily lost their active sites leading to deterioration of catalytic activity of maghemite/Cu/Pd for catalytic reduction of nitrite [22].

Dissolution of Cu and Pd from the bimetallic catalyst surface was measured by ICP-MS after each reaction cycle to check an extent of metal leaching. Negligible amount of leaching for precious metals (Pt and Pd) have been reported [18], while relatively higher amount of leaching for Cu has been reported during the reduction of nitrate by bimetallic catalysts supported with activated carbon (18.1%), carbon nanotube (15.9%) [26], silica oxide (10.6%), alumina (30.7%), and zirconium oxide (26.0%) [36]. However, maghemite/Cu/Pd showed no leaching of Pd throughout the three cycles and only 1.5% leaching of Cu from the first recycle with no detection of Cu leaching from the rest of two reaction recycles. This result confirms that maghemite/Cu/Pd exhibited an excellent stability and durability to strongly bind the bimetals on maghemite surface which can be a great advantage for its recycling for continuous catalytic nitrate reduction.

3.4. Reaction mechanism of catalytic nitrate reduction by maghemite/Cu/Pd

Catalytic nitrate reduction by bimetallic catalysts is significantly dependent on consecutive reactions induced by the bimetals (e.g., Cu and Pd) [50]. XPS analysis was performed to investigate change in oxidation state of Cu and Pd on the surface of maghemite/Cu/Pd before and after the nitrate reduction (Fig. 13). Dotted and solid lines represent original XPS analysis data and fitted line, respectively. Fig. 13 shows narrow scan of Cu(2p) and Pd(3d) on maghemite/Cu/Pd surface. The binding energy of 327.5–347.5 eV and 928–938 eV were used to identify oxidation state of Pd and Cu, respectively [23,55]. Clear peak at 932.4 eV was observed in Fig. 13(a)1, which is attributed to Cu(0) [23]. This indicates only Cu(0) was present on the maghemite/Cu/Pd surface before the nitrate reduction. After the nitrate reduction, two additional peaks at 931.1 and 933.9 eV appeared along with Cu(0) on the surface of maghemite/Cu/Pd, which were identified as Cu_2O and CuO, respectively (Fig. 13(a)2) [23,55]. XPS analysis data verifies that Cu(0) was subsequently oxidized to Cu_2O and CuO during the nitrate reduction. Based on the change in the oxidation state of Cu, the pathway of nitrate reduction can be explained by the following reactions:

$$NO_3^- + 2Cu(0) \rightarrow Cu_2O + NO_2^- \quad (7)$$

$$NO_3^- + Cu_2O \rightarrow 2CuO + NO_2^- \quad (8)$$

Nitrate was firstly adsorbed on the surface of Cu and reduced to nitrite by electron transfer from Cu(0). Cu(0) was oxidized to Cu_2O after the nitrate reduction and Cu_2O transferred electron to adsorbed nitrate for further nitrate reduction, resulting in the formation of CuO [23,55,56]. Nitrite is then desorbed from the surface of Cu for subsequent reduction to ammonium or nitrogen gas by hydrogen molecules [21]. Fig. 13(b) shows the oxidation state of Pd before and after the nitrate reduction by maghemite/Cu/Pd. Two obvious peaks at 335.7 and 340.9 eV did not significantly changed before (Fig. 13(b)1) and after (Fig. 13(b)2) the reaction. These two peaks are assigned to Pd(0) [23] indicating that oxidation state of Pd did not change during the nitrate reduction. Noted is that any electron transfers from Pd(0) did not occur during the nitrate reduction in this study because Pd(0) was only used to provide active sites for capturing hydrogen molecules [50]. Therefore, the pathway of nitrite reduction by maghemite/Cu/Pd can be proposed as follows [57]:

$$2NO_2^- + 4H_{ads}\text{-Pd}(0) \rightarrow Pd(0) + N_2 + 4OH^- \quad (9)$$

$$2NO_2^- + 12H_{ads}\text{-Pd}(0) \rightarrow Pd(0) + 2NH_4^+ + 4OH^- \quad (10)$$

Nitrite was reduced to ammonium or nitrogen gas by recombination of nitrogen atoms via hydrogen molecules adsorbed on active sites of Pd(0). Nitrogen gas can be formed from the reduction of nitrite when optimal amount of hydrogen molecules was provided (Eq. (9)), otherwise ammonium was likely to form with

excessive amount of hydrogen molecules (Eq. (10)) [58]. This indicates that the amount of hydrogen molecules accessible to the reduction of nitrite is a key factor to determine selectivity of nitrogen gas and ammonium in the catalytic nitrate reduction by maghemite/Cu/Pd.

4. Conclusion

Efficient, stable, durable, and eco-friendly bimetallic catalyst was synthesized using maghemite with Cu and Pd to selectively reduce nitrate to nitrogen gas. XRD analysis confirmed thermal transformation of lepidocrocite to maghemite, and SEM/EDX images demonstrated the uniform distribution of Cu and Pd particles on maghemite surface. maghemite/Cu/Pd showed higher removal (99.5%) in nitrate reduction than hematite/Cu/Pd (63%) and alumina/Cu/Pd (43%). The results obtained from parametric experiments varying Cu/Pd loading and hydrogen flow rate suggest significant key factors for the maximization of nitrogen gas selectivity, i.e. (1) optimal proximity between Cu (0.5 wt.%) and Pd (0.5 wt.%) for efficient hydrogen spillover, and (2) appropriate Pd (0.25 wt.%) loading and hydrogen flow rate (100 and 200 cc/min) to avoid accumulation of excessive hydrogen molecules. Recycling test of maghemite/Cu/Pd showed efficient nitrate reduction (>83%) with 33% of average nitrogen gas selectivity throughout three reaction cycles confirming its proper reusability. Pd leaching was not detected during three reaction cycles, while very low content of Cu (1.5%) was leached out only after first reaction cycle. The reaction mechanism of catalytic nitrate reduction by maghemite/Cu/Pd verified by XPS analysis can be explained by two-steps; (1) reduction of nitrate to nitrite is coupled with oxidation of Cu(0) to CuO, (2) nitrite is subsequently reduced to nitrogen gas or ammonium by hydrogen molecules adsorbed on the active sites of Pd(0).

Acknowledgements

This work is financially supported by the Korean Ministry of Environment (GAIA Project), National Research Foundation of Korea Grant funded by the Korean Government (MEST) (NRF-2012-C1AAA001-M1A2A2026588), and Korean Ministry of Land, Transport, and Maritime Affairs (U-City Master and Doctor Course Grant Program).

References

[1] B.T. Nolan, B.C. Ruddy, D.R. Helsel, Environmental Technology 31 (1997) 2229–2236.
[2] A. Pintar, Catalysis Today 77 (2003) 451–465.
[3] D.C. Bouchard, M.K. Williams, R.Y. Surampalli, J. Am, Water Works Association 84 (1992) 85–90.
[4] L.W. Canter, Nitrates in Groundwater, CRC Press, Boca Raton, 1996.
[5] M.P. Maia, M.A. Rodrigues, F.B. Passos, Catalysis Today 123 (2007) 171–176.
[6] H. Constantin, M. Fick, Water Research 31 (1997) 583–589.
[7] L. Knobeloch, B. Salna, A. Hogan, J. Pstle, H. Anderson, Environmental Health Perspectives 108 (2000) 675–678.
[8] D. Majumdar, N. Gupta, Indian Journal of Environmental Health 42 (2000) 28–39.
[9] H.H. Tsai, V. Ravindran, M.D. Williams, M. Pirbazari, Journal of Environmental Engineering and Science 3 (2004) 507–521.
[10] J.P. van der Hoek, P.J.M. van der Ven, A. Klapwijk, Water Research 22 (1988) 679–684.
[11] P.S. Barker, P.L. Dold, Water Research 30 (1996) 769–780.
[12] B.U. Bae, Y.H. Jung, W.W. Han, H.S. Shin, Water Research 36 (2002) 3330–3340.
[13] A.C.A de Vooys, R.A. van Santen, J.A.R. van Veen, Journal of Molecular Catalysis A: Chemical 154 (2000) 203–215.
[14] J.J. Schoeman, A. Steyn, P.J. Scurr, Water Research 30 (1996) 1979–1984.
[15] Y.H. Hwang, D.G. Kim, H.S. Shin, Journal of Hazardous Materials 185 (2011) 1513–1521.
[16] K.D. Vorlop, T. Tacke, Chemie Ingenieur Technik 61 (1989) 836–837.
[17] Y.H. Liou, S.L. Lo, C.J. Lin, C.Y. Hu, W.H. Kuan, S.C. Weng, Environmental Science and Technology 39 (2005) 9643–9648.
[18] L. Calvo, M.A. Gilarranz, J.A. Casas, A.F. Mohedano, J.J. Rodriguez, Industrial and Engineering Chemistry Research 49 (2010) 5603–5609.
[19] K. Daub, G. Emig, M.J. Chollier, M. Callant, R. Dittmeyer, Chemical Engineering Science 54 (1999) 1577–1582.
[20] U. Prüsse, K.D. Vorlop, Journal of Molecular Catalysis A 173 (2001) 313–328.
[21] Y.H. Liou, C.J. Lin, S.C. Weng, H.H. Ou, S.L. Lo, Environmental Science and Technology 43 (2009) 2482–2488.
[22] Y. Xie, H. Cao, Y. Li, Y. Zhang, J.C. Crittenden, Environmental Science and Technology 45 (2011) 4066–4072.
[23] W. Gao, N. Guan, J. Chen, X. Guan, R. Jin, H. Zeng, Z. Liu, F. Zhang, Applied Catalysis B 46 (2003) 341–351.
[24] O.S.G.P. Soares, J.J.M. Órfão, J. Ruiz-Martínez, J. Silvestre-Albero, A. Sepúlveda-Escribano, M.F.R. Pereira, Chemical Engineering Journal 165 (2010) 78–88.
[25] Y.X. Chen, Y. Zhang, G.H. Chen, Water Research 37 (2003) 2489–2495.
[26] O.S.G.P. Soares, J.J.M. Órfão, M.F.R. Pereira, Desalination 279 (2011) 367–374.
[27] R.H. Baughman, A.A. Zakhidov, W.A. de Heer, Science 297 (2002) 787–792.
[28] X. Zhu, Y. Chang, Y. Chen, Chemosphere 78 (2010) 209–215.
[29] A. Simon-Deckers, B. Gouget, M. Mayne-L'Hermite, N. Herlin-Boime, C. Reynaud, M. Carrière, Toxicology 253 (2008) 137–146.
[30] W. Lin, Y.W. Huang, X.D. Zhou, Y. Ma, Toxicology and Applied Pharmacology 217 (2006) 252–259.
[31] P.I. Girginova, A.L. Daniel-da-Silva, C.B. Lopes, P. Figueira, M. Otero, V.S. Amaral, E. Pereira, T. Trindade, Journal of Colloid and Interface Science 345 (2010) 234–240.
[32] J. Chomoucka, J. Drbohlavova, D. Huska, V. Adam, R. Kizek, J. Hubalek, Pharmacological Research 62 (2010) 144–149.
[33] S. Gyergyek, D. Makovec, A. Mertelj, M. Huskić, M. Drofenik, Colloids and Surfaces A 366 (2010) 113–119.
[34] R.M. Cornell, U. Schwertmann, The Iron Oxides, Structure, Properties, Reactions, Occurrences and Uses, second ed., VCH, Weinheim, 2003.
[35] W. Lee, G. Bae, Environmental Science and Technology 43 (2009) 1522–1527.
[36] Y. Yoshinaga, T. Akita, I. Mikami, T. Okuhara, Journal of Catalysis 207 (2002) 37–45.
[37] S. Bae, W. Lee, Geochimica et Cosmochimica Acta 85 (2012) 170–186.
[38] V. Bolis, B. Fubini, S. Coluccia, E. Mostacci, Journal of Thermal Analysis and Calorimetry 30 (1985) 1283–1292.
[39] T. Tuutijärvi, J. Lu, M. Sillanpää, G. Chen, Journal of Hazardous Materials 166 (2009) 1415–1420.
[40] S. Bae, W. Lee, Applied Catalysis B 96 (2010) 10–17.
[41] C.M. Mendez, H. Olivero, D.E. Damiani, M.A. Volpe, Applied Catalysis B 84 (2008) 156–161.
[42] R. Gavagnin, L. Biasetto, F. Pinna, G. Strukul, Applied Catalysis B 38 (2002) 91–99.
[43] H.E.L. Bomfim, A.C. Oliveira, M.C. Rangel, Reaction Kinetics and Catalysis Letters 80 (2003) 359–364.
[44] O.J. Wimmers, P. Arnoldy, J.A. Moulijn, Journal of Physical Chemistry 90 (1986) 1331–1337.
[45] O.S.G.P. Soares, J.J.M. Órfão, M.F.R. Pereira, Applied Catalysis B 102 (2011) 424–432.
[46] E.J. O'Loughlin, P. Larese-Casanova, M. Scherer, R. Cook, Geomicrobiology Journal 24 (2007) 211–230.
[47] J. Choi, B. Batchelor, C. Won, J. Chung, Chemosphere 86 (2012) 860–865.
[48] T.C. Zhang, Y.H. Huang, Journal of Environmental Engineering – ASCE 131 (2005) 461–470.
[49] F. Rodriguez-Reinoso, Carbon 36 (1998) 159–175.
[50] F. Zhang, S. Miao, Y. Yang, X. Zhang, J. Chen, N. Guan, Journal of Physical Chemistry C 112 (2008) 7665–7671.
[51] K.C. Waugh, Catalysis Today 15 (1992) 51–75.
[52] J.T. Sun, I.S. Metcalfe, M. Sahibzada, Industrial and Engineering Chemistry Research 38 (1999) 3868–3872.
[53] Z. Huang, F. Cui, H. Kang, J. Chen, X. Zhang, C. Xia, Chemistry of Materials 20 (2008) 5090–5099.
[54] R. Burch, C. Paun, X.M. Cao, P. Crawford, P. Goodrich, C. Hardacre, P. Hu, L. McLaughlin, J. Sa, J.M. Thompson, Journal of Catalysis 283 (2011) 89–97.
[55] J. Papavasiliou, G. Avgouropoulos, T. Ioannides, Journal of Catalysis 251 (2007) 7–20.
[56] F. Epron, F. Gauthard, C. Pineda, J. Barbier, Journal of Catalysis 198 (2001) 309–318.
[57] O.M. Ilinitch, L.V. Nosova, V.V. Gorodetskii, V.P. Ivanov, S.N. Trukhan, E.N. Gribov, S.V. Bogdanov, F.P. Cuperus, Journal of Molecular Catalysis A: Chemical 158 (2000) 237–249.
[58] W. Sun, Q. Li, S. Gao, J.K. Shang, Applied Catalysis B 125 (2012) 1–9.